J. Himalayan Ecol. Sustain. Dev. Vol 18 (2023) **ISSN 0973-7502**

Assessing Landslide Stability: Integrating Geophysical, Geochemical, and Geotechnical Approaches for Bioengineering Mitigation

Sunanda Patial[1,4], Vishvajit Kumar[2], Harsh Sharma[1], Ambrish Kumar Mahajan[1*], Pawan Kumar[3], Alok Kumar Pandey[1] and Sushma Negi[4]

[1]Department of Environmental Sciences, Central University of Himachal Pradesh, Dharamshala-176215, India
[2]Forest Research Institute, Dehradun, India
[3]Regional Research Centre, Chandsoli, Maharana Pratap Horticultural University, Karnal, Haryana-134203, India
[4]Department of Environmental Sciences, Maharaja Agarsen University, Baddi, District Solan, Himachal Pradesh- 174103, India
Corresponding author Email: akmahajan@rediffmail.com.

ABSTRACT

The Soldha landslide caused significant devastation to property and agricultural land on October 23, 2013, due to heavy rainfall, which triggered the slope failure. Nevertheless, substantial precipitation occurred in the slide zone between July and October 2013, resulting in significant moisture retention within the slide body. This, in turn, led to a decrease in shear strength and ultimately triggered the mass movement on October 23, 2013, thus threatening a large number of resident's downslope in the area. In order to evaluate the landslide and suggest possible mitigation measures, three techniques have been used, i.e. geophysical, geotechnical and geochemical. The ambient noise measurements (horizontal-to-vertical spectral ratio analysis) helped to estimate the slip geometry of slide zones whose depth varies from 15 m (near the scarp) to 45 m (centre) along the slide slope. The LiDAR survey reveals that the slides are active and have movement in the order of 0.032 m in the northwest side to 0.398 m in the southeastern direction. The chemical analysis suggests a robust spatial dependency correlation between different soil parameters like zinc (Zn), nitrogen (N), iron (Fe), copper (Cu) and phosphorus (P), except organic carbon (OC), manganese which has a week to moderate spatial dependency. Thus, the combination of different methods allows an understanding of the directional nature of the slide zone, depth of the slip surface, rate of movement, grain size percentage, water holding capacity of soil and dependence of the soil on different elements, allowing for bioengineering measures.

Keywords: *Slip Geometry, Ambient Noise Measurements, Chemical analysis, Bioengineering, Disaster risk reduction*

INTRODUCTION

During the monsoon season, every year, the Himalayan terrain witnesses slope destabilisation events, causing losses in material damage worth crores of rupees. By anticipating the causes of slope failures and providing mitigation measures which can be site-specific, one can alleviate the risk. Currently, several geophysical and geotechnical methods are in practice to investigate any slide zone's internal properties, slope dynamics and mechanical properties to provide a complete understanding of the effective behaviour of any soil mass (Del Gaudio *et al.,* 2014; Le Breton, 2019; Guillemot *et al.,* 2020). Amongst different geophysical methods, the sensitivity of the electrical process is more towards estimating the pore water salinity and water circulation due to the conductive nature of water (Jongmans and Garambois, 2007; Whiteley

et al., 2019). However, active and passive seismic methods using microtremors and seismic reflection techniques offer a direct perception of the mechanical alteration of near-surface material that can cause failure.

Out of these two methods, a passive seismic method using ambient noise measurements also named horizontal-to-vertical ratio (HVSR) has been extensively used in the past for various applications, including site characterisation, site amplification, landslide zonation by mapping of the fractures and unstable regions, and earthquake-induced slides (Nakamura, 1989; Del Gaudio *et al.,* 2014; Le Breton, 2019; Guillemot *et al.,* 2020; Mahajan *et al.,* 2021; Patial *et al.,* 2023). The ambient noise measurements were taken using small microtremor instruments (Tromino) by placing them at least 1ft down in the ground to avoid any disturbance from the wind noise. The idea is to record passive noise to record high-resolution digital seismic data of low-frequency waves (Nakamura, 1989). Presently, several studies related to HVSR analysis have been increasing not only in the field site characterisation but also in evaluating landslides and understanding their dynamics to reduce by detecting a decrease in apparent seismic velocity before to the failure of landmass (Del Gaudio *et al.,* 2014; Kleinbrod *et al.,* 2019; Breton *et al.,* 2021). The primary significance of the technique is that it allows us to understand the drop in shear wave velocity with depth, which is indicative of a reduction in rigidity in an underground layer, which in turn associated with the failure of the slide zone (Imposa *et al.,* 2017; Pazzi *et al.,* 2017; Bontemps *et al.,* 2020; Fiolleau *et al.,* 2020; Patial *et al.,* 2023).

It is well known that the Outer Himalayan foothills are tectonically active and prone to landslide activity due to heavy rains during monsoon, leading to erosion and deposition of sediments (Mahajan *et al.,* 2010; Singh and Awasthi, 2019; Mahajan *et al.,* 2022; Singh *et al.,* 2022). The northwest Himalayan region is also seismically active and has witnessed significant and moderate earthquakes from time to time in past (Narula and Shome, 1992; Ambraseys and Bilham, 2000; Kumar and Mahajan, 2001; Mahajan *et al.,* 2010). Further, the equilibrium stage of geomorphological features and denudation of unstable and fragile hills due to neo-tectonic activities further accelerate the landslide movements in the frontal part of the Himalayas (Sharma and Mahajan, 2020). The continued northward journey of the Indian subcontinent also enhances the tectonic activities, which increases strain accumulation, thus increasing the slope failure vulnerability since the bulk population resides in the outer Himalayan area, which is susceptible to significant disasters during monsoon seasons (Anbalagan, 1992; Thakur *et al.,* 2014), therefore apply bioengineering application could prove to be fruitful.

In the Himalayan region alone, more than 15% of the land area is being affected due to landslides covering more than 0.49 million km2. Himachal Pradesh is one such area in northwest Himalaya that suffered 5502 landslides, 27 cloud bursts, and 83 flash floods thus affecting 201 villages (s*ource: Received from District Emergency Operation Centre)*) in whole of Himachal during 2023 monsoon season (*Source: Received from State Emergency Operation Centre, Himachal Pradesh)* causing a loss of 9905.77 crores of rupee to the infrastructure and agricultural land (*source:*

State disaster Management authority, Himachal Pradesh). The Soldha slide zone is one such area in the Kangra district of Himachal Pradesh (India), which was also reactivated and covered a large part of the landmass subjected to movement. The slide zone was also monitored from 3-5 November 2023 using a terrestrial Lidar survey as experimental studies were being conducted by Mr Sayed Hyder Ali, M/s Meatech Solution, Gurgaon, and continuous observation was taken for three days.

This research explores the effectiveness of bioengineering measures in mitigating erosion. The selection of suitable plants for erosion control and restraining further downslope movement of the landmass is informed by the analysis of subsoil chemical properties, slip surface depth, and lithology using geological and geophysical methods, as detailed earlier. Mitigating the risks associated with both pre- and post-landslides necessitates mapping landslide-prone areas. Subsequently, appropriate mitigation measures, be they physio-mechanical engineering (geotechnical) or bioengineering approaches, are implemented based on factors such as lithology, slope characteristics, and the area's significance, encompassing strategies like slope soil stabilization and the construction of retaining walls.

As highlighted by Lan *et al.* (2020), the efficacy of tree plantation in reinforcing slopes is notably higher at angles of 20 and 35 degrees when compared to slopes ranging from 50 to 60 degrees. Gray and Leiser (1982) emphasize the significant impact of herbaceous vegetation, and to a lesser extent, woody vegetation, in effectively controlling landslides and mass movements. Adding to this perspective, Vasistha *et al.* (2011) point out that plant-induced depletion of soil moisture content plays a crucial role in delaying saturation and runoff, thereby mitigating the risk of mass movement. Additionally, the mechanical reinforcement provided by roots contributes to soil stability by converting shear stress within the soil into tensile resistance within the roots.

STUDY AREA

The Soldha slide zones fall to the north of Niangal village district Kangra, form a part of the Bhed watershed, and fall in SOI toposheet no 52D/3 (Fig.1). This slide zone is situated in the sub-humid climate of the Kangra region thus, experiences maximum rainfall during the monsoon season, spanning from July to September. The Soldha landslide zone is an integral part of the Bhed Khad watershed, where all tributaries converge into the Beas River basin. It falls within the sub-humid regime, receiving an annual rainfall of up to 1750 mm, primarily concentrated in the monsoon months. Extending over 0.78 km along the displaced hillock, the landslide zone covers an area of 0.25 km², exhibiting altitudinal variations from 715 m at the toe to 977 m at the scarp zone (Fig. 2)

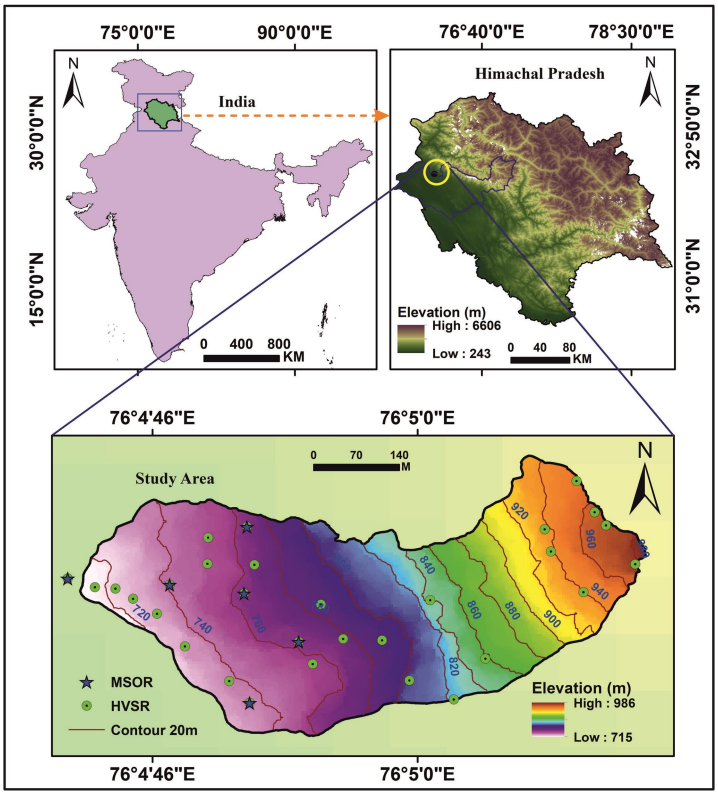

Fig. 1.Shows the location of Soldha slide zones (lower picture) in Himachal Pradesh, India. The location of the site covered under Horizontal-to-vertical spectral ratio (HVSR) analysis as green circles and multiple simulations with one receiver (MSOR) as a star are shown along with a contour interval of 20 m and elevation variation from 715 m (violet) to 986 m (dark mustard colour).

The Soldha landslide was triggered early on the 23rd of October, 2023. The region has been experiencing very high rainfall episodes since July 2013, which might have increased soil mass saturation level and reduced shear strength. The slide zone had developed alarming features such as surface cracks and land fissures, which allowed the villagers to move out before 23rd October night and save their lives. Geologically, the slide zone is situated on the hanging wall of the Jawalamukhi Thrust, acting as the division between the Middle Siwalik sandstone to the north and the Upper Siwalik Conglomerates to the south. Within the landslip area, the geological composition is characterized by Middle Siwalik Sandstone with clay intercalations, and the predominant surface material in the slide zones comprises rock fragments of buff-colored sandstone along with intercalations of clay stones. The slopes predominantly face southward, and the southern section of the slide zone is draped in debris material sourced from the first and second detachment zones of the slide, as documented by Mahajan *et al.* (2022).

The slide is very steep at the crown part and has moderate slopes in the lower part, with elevation variations from 715 m at the toe to 977 m at the crown region within a distance of 0.78 km. The slope gradient along section A' (inset) indicates steeper slopes with break-in slopes at different parts of the slide zones. Fig. 2 shows the general

trend of the hill at various parts of the slide zone. The detachment zones at the crown and first scarp and the areas with debris material at different parts of the slide zone are shown along the elevation profile.

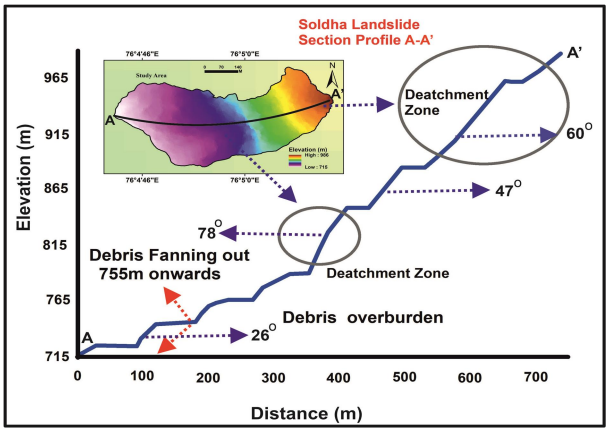

Fig. 2. Cross section of the slide zone depicting elevation variation along the A-A' section

This Soldha landmass moved downslope in two different stages; initially, the first scarp was developed a few meters down the crown portion, followed by the movement along the crown region, as stated by Mahajan *et al.,* 2022. Lithologically, the landslide mass comprises sandy soil with weathered rock from the scarp region, gullies and uneven topography.

Fig. 3. Shows lithological characteristics of the slide zone: a) The area on the left of the slide zone, which was exposed due to the activity in the region; b) shows the presence of weathered rock material from the scarp region; c) the central part of the slide zones in the western side indicating weathered soil with uprooted trees and bushes, d) uneven topography on the southeast part of the slide in the slide zone with sandy to fine soil particles.

The material derived from the slide movement seems vast. It has a deeper slip surface that displaces physical and anthropogenic elements (houses, forest cover, etc.) by 40-60 m down the slope in different directions (Mahajan *et al.,* 2022). Simultaneously, a large chunk of the landmass comprising highly jointed sandstone was exposed, and a prominent bend or scar developed in the western part of the slide zone (Fig. 3a).

This study area contained precarious slopes at the scarp, although it stabilized a little after the deposition of eroded soil and rocks/debris at the middle and lower parts of the slide. During the investigation, stones and soil failure positions are documented as joints. The slide has resulted in large gullies, the undulatory nature of landmass and large-scale crevasses. The slide zone's crown part and western sides have rock exposures - which are highly jointed—the rock exposures of sandstone lie in different degrees of weathered conditions. The region's highly deformed and jointed rocks reflect the presence of geological discontinuities south of slide zones. According to various authors' investigations, minor earthquakes in the last few years have also made this area vulnerable to movement (Kumar and Mahajan, 2001; Mahajan *et al.,* 2022).

MATERIAL AND METHODS

Rainfall Data Analysis

The temporal variation in rain intensity was analyzed using daily precipitation data (TRMM—near-real-time) from August 2013 to October 2013 (Fig. 4). The precipitation data unveiled an unusual spike in rainfall during the second week of October 2013, just preceding the triggering of the Soldha landslide. This event unfolded following substantial rainfalls in August and September, with an additional peak in October (Fig. 4).

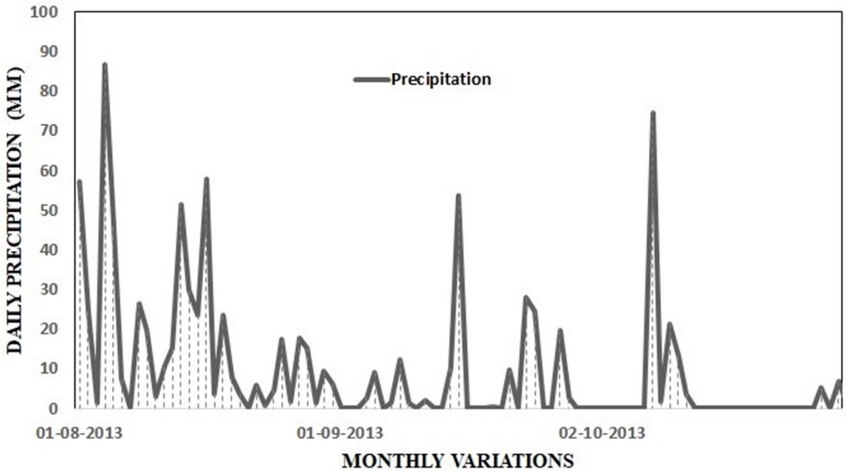

Fig.4. Shows rainfall data and intensity of rainfall prior to the landslide in October 2013 (Data Source: NASA (TRMM) satellite data)

Joint Analysis

Joints, lineaments, discontinuities, and rock orientation control the failure of rock/debris and overall slope stability. Therefore, to understand the geometry of the failure, a kinematic analysis [KA] has been performed to determine the failure type of rock slopes near the crown, the western edge of the slide zones and the direction of the joints/shear zones. During the field visit, data on shear zones and joints were collected and analyzed into stereographic projections to identify the intersection lines. The joint data was collected from the crown region and along the national highway, where rock exposures were observed. The idea was to have a few samples near the highway since it is close to the Jawalamukhi Thrust (sites 10 and 11) to understand the general trend of the joints in the region, whereas sites 1-8 were from the slide zone. The analysis reveals that four areas in the slide zone are highly jointed with minor shear zones [site no. 01, 03, 04 and 05] (Fig. 5). They are unstable, and site-02 is complexly joined with damp water conditions. However, site no. 01, 05 and 08 have apparent failure related to the wedge.

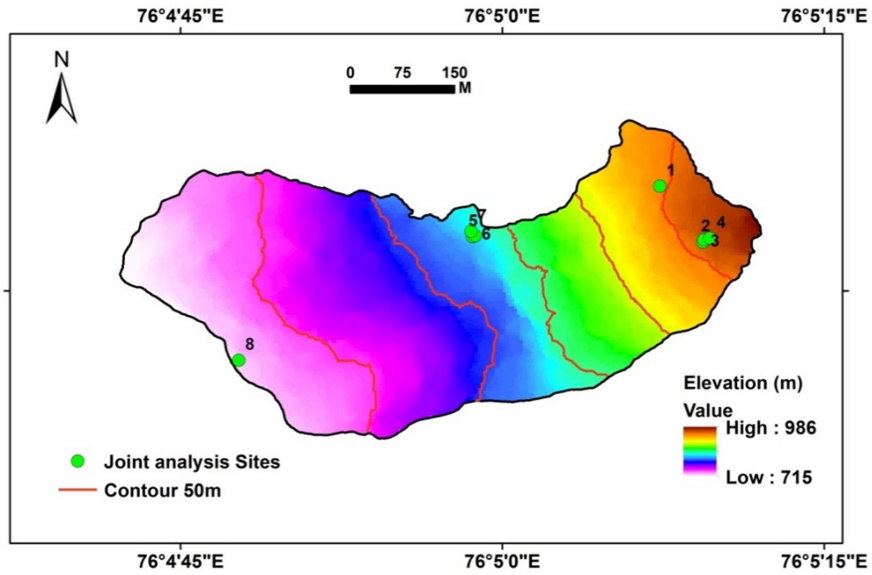

Fig. 5. Shows the location of joints reading in the Soldha slide zone. The readings were taken only from the areas where rocks were exposed. Rest of the area was covered with debris material.

In contrast, sites 02, 03, 04, 06, and 07 are planer failures or mostly complex due to the geo-tectonic factors (Mahajan *et al.,* 2022). In most places, a minimum of five to six sets of joints responsible for a failure's complexity have been identified. All types of losses, viz planar, wedge, and complex planes, were determined from the analysis of stereo plots, especially in rocky areas (Fig.6). The rockslide, coupled with debris mass, forms the primary material of the slide zones.

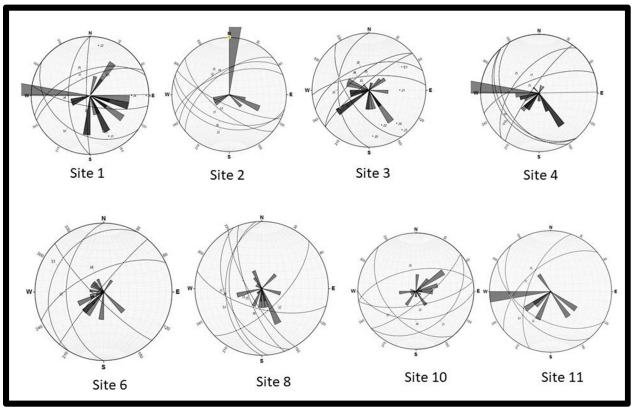

Fig. 6. Shows joints analysis from the slide zones where rocks are exposed indicating multidirectional joints thus reflecting tectonic complexity of the area

Monitoring of the Soldha slide zone using Terrestrial LiDAR Survey- an experimental study

The Soldha slides zone was reactivated after ten years and has shown substantial movement in the slide area with the direction of movement on the south-eastern side (Fig.7). The rate of movement was found to be very active and to monitor the rate of movement, a terrestrial LiDAR survey has been designed in the area and slide was monitored for three days**.**

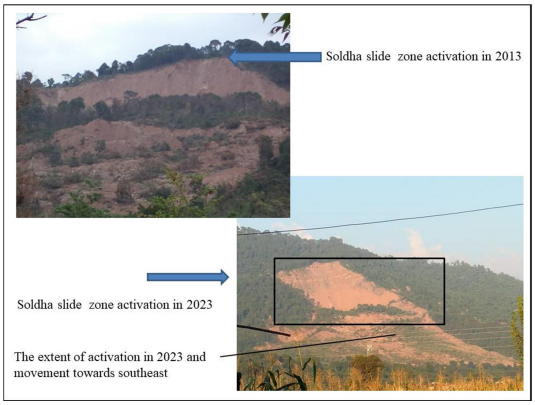

Fig. 7. Shows the reactivation of the Soldha slide zone during 2023 monsoon after a gap of ten years that lead to movement in the large area of Niangal village. The extent of the damage caused due to mass movement in 2013 and 2023 has also been shown.

Terrestrial LiDAR Survey

Terrestrial LiDAR (Light Detection and Ranging) survey is a powerful technique based on principal of 'Times of Flight' that uses laser light to measure distances and create detailed, three-dimensional representations of the Earth's surface. This method provides highly accurate and dense point cloud data, making it a valuable tool for various applications (Slob and Hack 2004; Jaboyedoff *et al.,* 2009).

Data acquisition

Terrestrial LiDAR systems consist of laser scanners mounted on tripods or other stable platforms. These scanners emit laser beams that bounce off surfaces and return to the sensor. The time the laser beams travel to the target and back is measured, allowing precise distance calculations. The collected distance measurements form a dense point cloud representing the surveyed area in three dimensions. Each point in the cloud corresponds to a specific location on the surface and is defined by its XYZ coordinates. Multiple scans are often necessary to cover larger areas. Registration aligns these scans into a single, cohesive point cloud. The registered point cloud can be integrated with other geospatial data, such as GPS or imagery, to enhance its accuracy and context (Carter *et al.,* 2001; Slob *et al.,* 2002; Haugerud *et al.,* 2003; Slob and Hack 2004).

Terrestrial LiDAR is widely used for creating highly accurate topographic maps, and built-in GPS and differential GPS help monitor the rate of movements on the surface. It captures detailed elevation information, including the shape and features of the terrain, which is crucial for understanding minor movements on the surface. In the present survey, the RIEGL VZ-2000i Terrestrial Laser Scanner is being used for data accusation, having a range of 2500 m with an accuracy of 5mm. The system has automatic on-board registration, including voxel extraction and merging scan position in the background to fasten the registration in open-pit mine surveying.

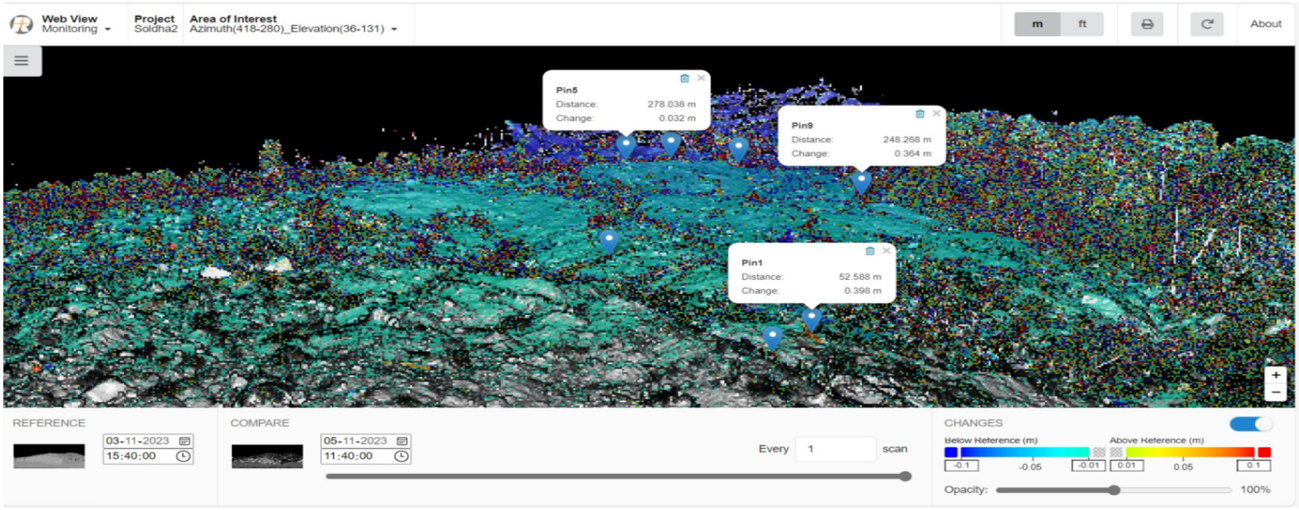

Fig. 8. Soldha (Himachal Pradesh) landslide's scan at 11:40 AM on 5th November 2023 after continuously monitoring the slide zone from 3th November, 2023. The values are highlighting the movements at various depicted places in 44 hours with respect to the reference scan. A total of 19 scans are taken. The rate of movement has been noticed which vary from 0.032m in the northwest side to 0.398 m in the south-eastern direction in 44 hrs indicating a very alarming rate of movement in the region.

Chemical Analysis of Soil

To estimate the macro and micronutrient content of the soil in and around the Soldha slide zone, 55 soil samples were collected from the slide area. The main idea of collecting these samples is to understand the overall fertility and health of soil, which enables us to identify suitable plant species that can used as bioengineering measures for holding soil particles and strengthening the soil from further movement (soil sample locations are shown in Fig. 9).

Laboratory studies

i. Soil parameters

Soil sampling

Upon concluding the experiment, soil samples (0-15 cm depth) were systematically gathered from representative sites (Fig.9). Following shade-drying, the samples underwent grinding in a pestle mortar, passed through a 2 mm sieve, and subsequently underwent laboratory analysis. The processed soil samples were examined for variations in pH, organic carbon, and the availability of N, P, and K.

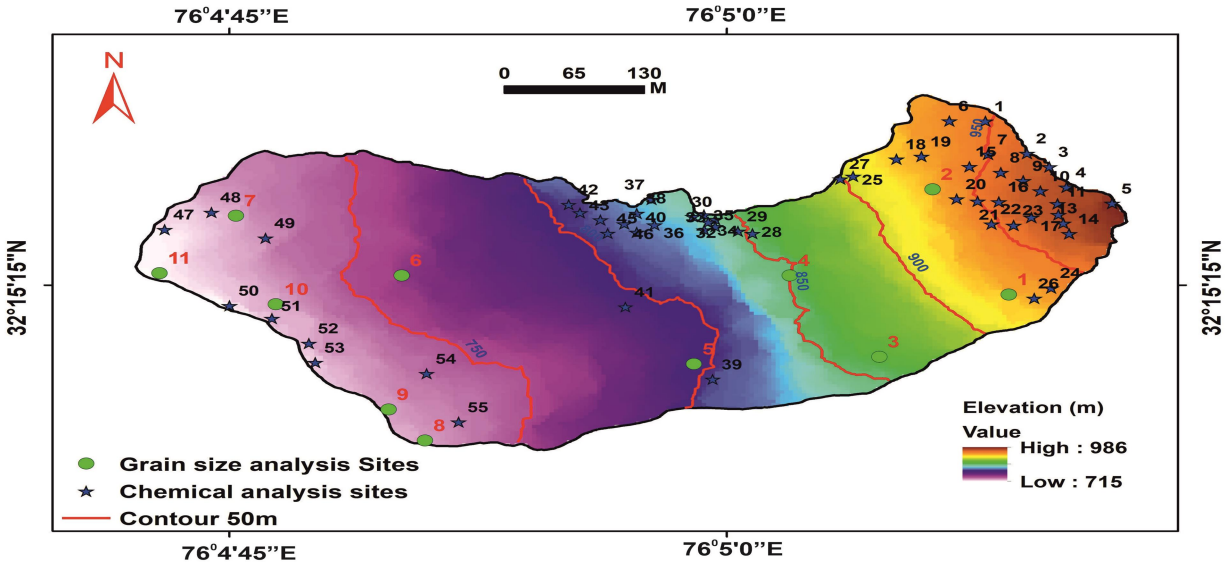

Fig. 9. Shows the soil samples collection sites for grain size and geochemical analysis for bioengineering applications

The pH of the soil was determined by mixing soil samples in distilled water in a ratio of 1:2.5, which allows it to extract the soluble components in the water (After that, the pH of the soil samples solution was determined using standardized and calibrated pH meter by using buffers of pH four and pH 9 to ensure the accuracy and reliability of the pH measurements (Jackson 1973). The pH solution represents the algorithm of the concentration of hydrogen ions, thereby providing valuable information on soil suitability for different plant species.

Organic carbon

The wet digestion method was followed for determination of organic carbon content from each soil sample (Walkley and Black, 1934).

Nitrogen

The available nitrogen content was determined using the alkaline permanganate ($KMnO_4$) method as outlined by Subbiah and Asija (1956).

To estimate nitrogen presence in soil samples (2.0 g each), the alkaline potassium permanganate method was employed. In this process, potassium permanganate ($KMnO_4$) was utilized to extract the nitrogen fraction from organic nitrogen. Initially, the samples were placed in Kjeldahl's distillation flask and moistened with distilled water. In a conical flask, 25 ml of a 2% boric acid solution was prepared, and the delivery tube's end from the distillation flask was carefully immersed in it. Subsequently, 100 ml of 2.5% sodium hydroxide (NaOH) and 100 ml of 0.32% $KMnO_4$ were added to the distillation flask, and a cork was tightly sealed to prevent ammonia gas loss. Finally, the boric acid solution containing ammonia was titrated against 0.02N H_2SO_4, and the endpoint was determined by the color change from bluish-green to pinkish-wine red.

Phosphorus

A 1 g soil sample was placed in a 100 ml plastic bottle, and a 20 ml bicarbonate extract, prepared following the Olsen method with 42g sodium carbonate and distilled water to achieve a volume of 1 liter, was employed. The sodium bicarbonate extraction method, as outlined by Olsen (1954), was utilized to evaluate available phosphorus in soils from the Soldha Landslide region. Following this, the ascorbic acid reductant method was implemented to measure phosphorus in the collected soil samples. This method entails the reduction of the ammonium phosphomolybdate [$(NH_4)3PO_4.12MoO_3$] complex by ascorbic acid ($C_6H_8O_6$) in the presence of antimony potassium tartrate [$K(SbO)C_4H_4O_6.½H_2O$], as elucidated by Kumar et al. (2019). Initially, 12 g of ammonium molybdate was dissolved in 250 ml of distilled water to create the stock solution, and 290.8 mg of [$K(SbO)C_4H_4O_6.½H_2O$] solution, prepared with 100 ml of distilled water, was added. To this solution, 1 liter of 5 N H_2SO_4 was introduced, and the final volume was adjusted to 2 liters using distilled water. Subsequently, a mixed reagent was formed by adding 200 ml of 1.056 g of L-ascorbic acid to the stock solution.

Potassium

Potassium content was determined through the flame photometric method, following the procedure outlined by Jackson (1973). A 5 g soil sample was utilized, and 50 ml of 1 N neutral ammonium acetate (CH_3COONH_4) was added. The mixture was allowed to stand undisturbed for 15 minutes, followed by placement on an electric shaker for an additional 5 minutes. Subsequently, the mixture was filtered using Whatman no-filter paper. The Flame Photometer instrument underwent calibration before individually running all prepared samples. Readings were recorded, and the final potassium concentration in kg/ha for each sample was calculated.

DTPA extraction

The DTPA-extractable Zn, Fe, Mn and Cu were measured with an atomic absorption spectrophotometer per the standard procedure outlined by many researchers (Lindsay and Norvell, 1978; Kumar *et al.,* 2021). The diethyl Triamine Penta acetic Acid (DTPA) method and the Atomic Absorption spectrophotometer (AAS) were used to determine the micronutrients. The samples were prepared by mixing DTPA, Tri-ethanolamine (TEA), and calcium dihydrate (CaCl2.2H2O) in soil samples to extract micronutrients. The pH of the solution thus designed was adjusted to 7.3 by adding 1N HCL. Finally, the centration of micronutrients was determined through AAS after due calibration.

Spatial dependency of different soil parameters

The variability and spatial relationship of various soil parameters to those mentioned above were

analysed using a semivariogram. The semivariogram reflects the means square variability among soil samples located close to each other within a distance 'h' is represented as under:

$$\gamma(h) = \frac{1}{2m(h)} \sum_{i=1}^{m(h)} [Z(X_i + h) - Z(X_i)]^2 \quad \text{..... [Eq-1]}$$

Where Z (Xi + h) represents the value of the soil parameter at two different sites (Xi and Xi + h), while m (h) represents the number of observation pairs separated by a distance 'h'.

To understand variability in the data, two models have been used: 1) the exponential model (eq-2) and the Gaussian model (eq. 3), as described in Kumar et al. (2021).

$$\gamma(h) = C_0 + C\left[1 - \exp\left(\frac{-h}{A_0}\right)\right] \text{.....[Eq-2]}$$

$$\gamma(h) = C_0 + C\left[1 - \exp\left(\frac{-h^2}{A_0^2}\right)\right] \text{..... [Eq-3]}$$

Where 'h' represents the lag interval, 'C' and 'C0' denote the structural variance (greater than or equal to C0) and the nugget variance (less than or equal to 0). The parameters' range (or degree) is indicated by 'A' (Reza *et al.,* 2019).

By undertaking statistical analysis of different soil parameters, their degrees of similarity for each soil parameter have been assessed by fitting the data either on the Exponential or Gaussian model. The information obtained is valuable in understanding patterns of soil properties across the slide zone, which has aided us in deciding the plant species to be planted at each site as bioengineering measures. According to the analysis, the soil is sandy, with organic carbon content ranging between 0.25 to 0.40 %, indicating low organic matter content that also affects soil fertility (Table-1).

Table 1. Shows spatial variability and degree of similarity among different soil parameters

Parameter	Model	Nugget (C_0)	Partial sill (C)	Sill (C_0+C)	Nugget/Sill (%)	Spatial dependency class	Root mean square error
OC	Gaussian	0.059	0.01	0.1	85.51	Week	0.257
N	Exponential	455.5	1494.1	1949.6	23.36	Strong	42.01
P	Exponential	0.03	83.41	83.4	0.04	Strong	8.56
K	Gaussian	8726.7	3396.1	12122.8	71.99	Moderate	101.3
Cu	Gaussian	0.158	1.984	2.1	7.38	Strong	1.41
Fe	Exponential	0.51	19987	19987.0	0.003	Strong	103.7
Mn	Gaussian	0.016	0.026	0.0	38.10	Moderate	0.167
Zn	Exponential	0.03	2.24	2.3	1.32	Strong	0.19

Geophysical Methods for Landslide Monitoring

Ambient noise measurements for landslide monitoring

Landslide risk in a hilly area can be reduced by anticipating slope failures by installing early warning systems; however, such methods are not well established in many regions, which can save the terrain from further loss. Under such circumstances, the slide zone's geophysical investigations and geological inputs were

required to understand the internal structure and near-surface material properties. Recently, several geophysical methods have proved to be effective for understanding near-surface material properties like depth of slip surface and hydrological parameters and to have insight into soil dynamics (Jongmans and Garambois, 2007; Whiteley *et al.,* 2019).

Amongst various geophysical methods, the electrical method is one such method which can be used to measure pore water salinity, water circulation and other hydrological parameters; however, measuring only groundwater level circulation and salinity will not provide information on rupture sediments thickness above competent strata (Carriere *et al.,* 2018). In contrast, the passive seismic method provides physical properties of the subsurface up to the slip surface and even allows us to observe the depth of the slip surface and direction component of the slide zone (Larose *et al.,* 2015; Patial *et al.,* 2023). According to various authors, the thickness of the impedance contrast between the overlying soft sediments and underlying stiff material can be understood by estimating resonance frequency and stiffness values with depth (Imposa *et al.,* 2017; Pazzi *et al.,* 2017). The spectral amplification of any site can be performed using the horizontal-to-vertical spectral ratio (HVSR) analysis method (Nakamura, 1989).

This technique has been established and used extensively for site characterisation and amplification studies. Recently, the same methods have also been used for mapping landslides, mapping fractures and unstable slopes by various authors (Del Gaudio *et al.,* 2014; Kleinbrod et al., 2019; Amitrano *et al.,* 2007; Meric *et al.,* 2007; Danneels *et al.,* 2008). According to the study, the ambient Noise measurements coupled with multiple simulations (passive seismic interferometry) can detect a drop in shear wave velocity and, in turn, a decline in rigidity in the underground layers, which thus can be used for predicting a landslide before a failure. Therefore, this method has been proven to have the potential for detecting slope failure (Burjanek *et al.,* 2010; Hausler *et al.,* 2019; Sens-Schonfelder and Brenguier, 2019).

Data acquisition and processing

Fig.1 shows the location of sites covered under ambient noise measurement (30 sites), and the instrument used was a three-component electro-dynamic sensor with a 0.1 –1024 Hz frequency range. To avoid wind noise and other anthropogenic noises, the device was placed in an almost 1ft bottomless pit to have a proper coupling of the recording unit. The data was recorded for 20 minutes, with a sampling frequency of 128 Hz per site effect assessment using ambient excitations (SESAME) guidelines. The acquired data were processed using Grilla software using 60 non-overlapping time windows of 20 sec with different smoothing parameters. The data processing was done in the frequency range of 0.2-30 Hz as this range covers the engineering interest and the presence of peaks due to thick sediments and boulders (included in debris material). Noises were filtered to get a clear spectrum, and the records were processed using a triangular smoothing window because anthropogenic noise may affect the HVSR curve below 2 Hz (Mahajan *et al.,* 2021).

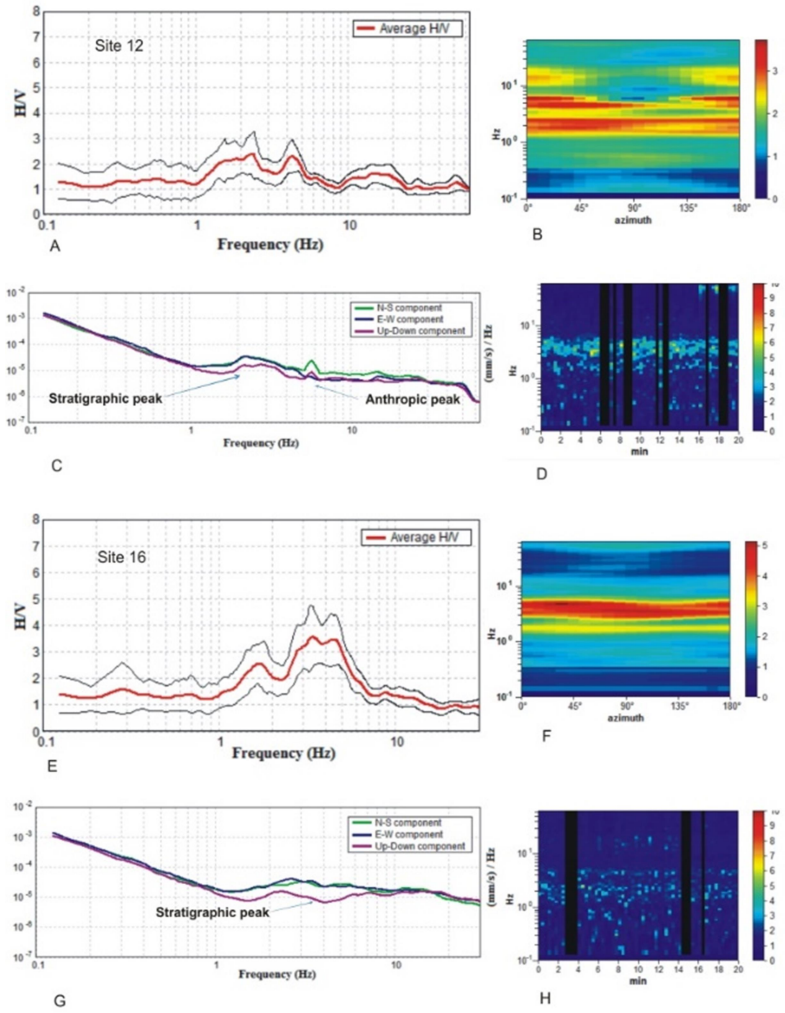

Fig. 10. Shows HVSR curves (A and E, site 12 and 16, respectively) with average curves in red colour directional response (B and E) stratigraphic peaks are represented in C and G with noise spectrum as D and H for site 12 and 16, respectively.

The data was processed in a frequency range of 0.2 to 30 Hz by removing noise to get a clear HVSR peak, directional response and noise spectrum (Fig. 10). The removal of noise from the data helped to distinguish between stratigraphic and anthropogenic peaks (Fig. 10 C and G). The sites with multiple fundamental frequency peaks (f_0) had distinctive frequencies, as shown in Fig.10A and 10E. The directional response shows moderate to gentle slope topography for sites 12 and 16, as the directional response will help understand the direction of mass movement (Patial *et al.,* 2023).

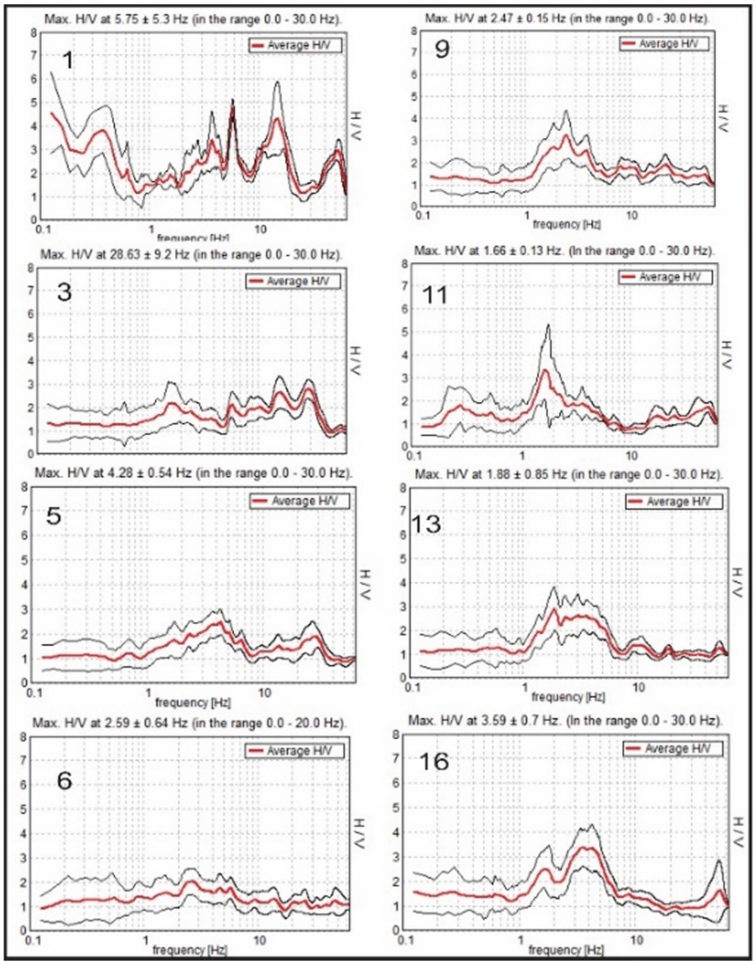

Fig. 11. HVSR curves of different sites indicating multiple peaks (site no 3, 5, 6 and clear peaks (site no. 1, 9, 11, 13, 16). The clear peaks have fundamental frequency 3-4 Hz, whereas the multiple peaks have frequency at 2, 4 and 10 Hz.

Processing and analysis of the HVSR peaks have been performed to define the reliability of the H/V peak and apparent H/V curve (SESAME, 2004; Rezaei *et al.,* 2013, 2017). Most sites have low-frequency (1-2 Hz) or mid-frequency (3-4 Hz) peaks, which have also been checked for conformity with SESAME criteria to identify layers of resonance and thickness of sediments. Some sites have low confidence levels concerning SESAME criteria, but 80% meet the criteria for clear HVSR peaks, and 90% have reliable HVSR curves (Fig 11 and 12).

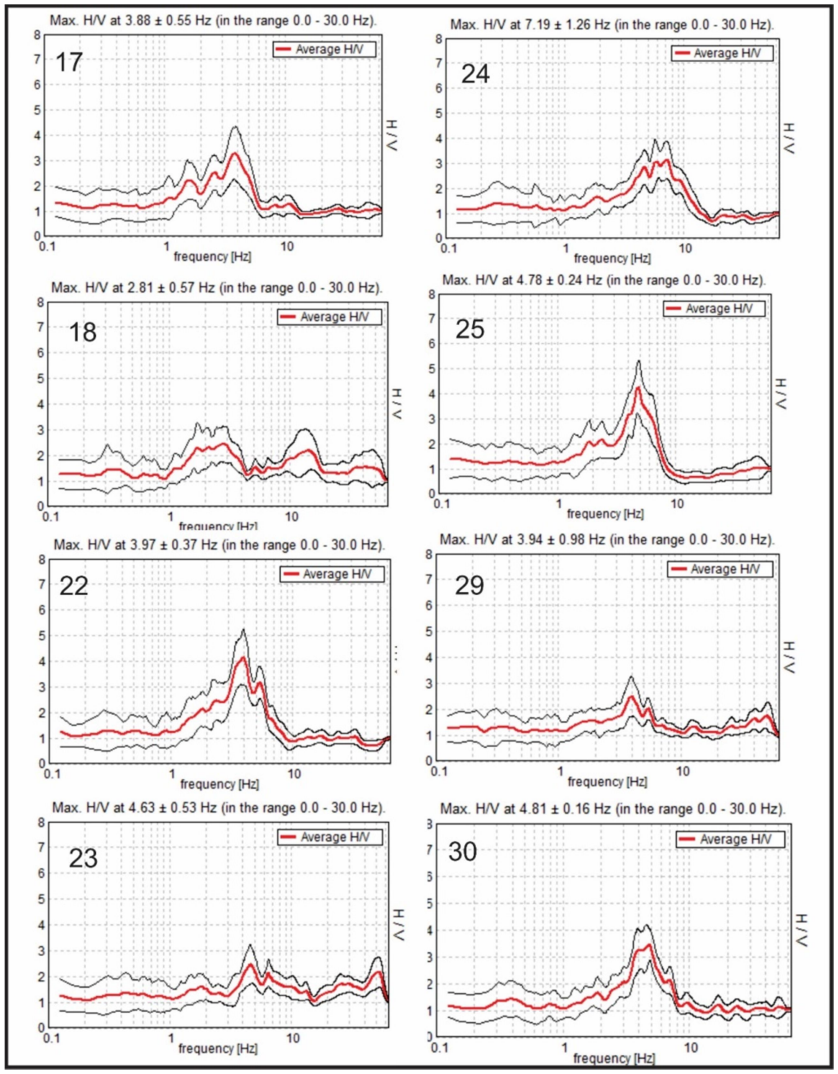

Fig. 12. HVSR curves of different sites indicating multiple peaks (site no 18, 23 and 29 and clear peaks (site no 17, 22, 24, 25 and 30). The clear peaks have fundamental frequency 3-4 Hz, whereas the multiple peaks have frequency at 2, 4 and 10 Hz indicating variation in stiffness and thickness of slide material.

Multichannel Simulation with One Receiver (MSOR)

Data Acquisition

An active seismic method was needed to obtain the near-surface material properties in terms of the shear wave velocity; however, looking at the sloping surface and the presence of debris material, it was challenging to have a linear profile in any of the sites on the Soldha slide zones. Therefore, multiple simulations have been obtained from each site covering a linear length of 15-20 m to get the surface information. The numerous simulations with one receiver using the same instrument (Tromino), which had been used for recording ambient noise, were used, whose methodology has been well explained in earlier publications (Mahajan *et al.,* 2021). The advantage of the MSOR method is that it can be employed in hilly terrain and an urban centre where getting a more extended linear profile is a

significant problem. On the other hand, it has the disadvantage that it cannot investigate soil properties below a few meters due to concise profile length; however, provided we have near-surface material properties, which are required for inverting HVSR curves to get 1-D shear wave velocity of that site.

On the other hand, the MASW technique provides high-resolution data on shear wave velocity profiles for the top 30-40 m but requires a longer linear profile length (100-150 m). This technique can provide independent shear wave velocity profiles compared to the MSOR technique, whose dispersion curves are used to invert HVSR curves to get the shear wave velocity of that site. Since it was impossible to run MASW profiling in the slide zone, the MSOR technique was used for the desired information.

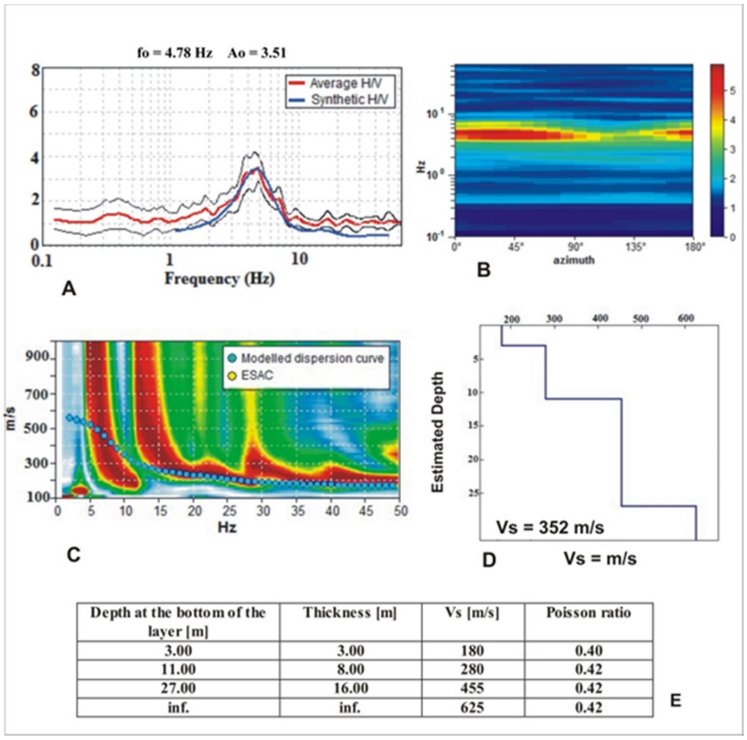

Depth at the bottom of the layer [m]	Thickness [m]	Vs [m/s]	Poisson ratio
3.00	3.00	180	0.40
11.00	8.00	280	0.42
27.00	16.00	455	0.42
inf.	inf.	625	0.42

E

Fig.13. Shows example of joint fit inversion from Soldha slide zone where A) shows HVSR curves with frequency (Hz) along x-axis and amplification (A) along Y-axis B) directional response with azimuth along x-axis and frequency along y-axis C) dispersion curves derived using MSoR technique with phase frequency (Hz) along x-axis and phase velocity (m/s) along y-axis D) 1- Velocity curve derived using HVSR curve and dispersion curves E) shows the tabular form of the 1-D velocity model reflecting thickness of the sediments below surface and their corresponding shear wave velocity (Vs) and poisons ratio.

The procedure proved to be one of the best methods in such areas where there were limitations to having linear profiles of 50-100 m length for obtaining the initial information of the shear wave velocity from the dispersion curve (Ryden *et al.,* 2004). Under this method, a sensor (recorder) was placed at one end, and a geophone from the recorder was placed at a distance of 1 m. The impact source was at a distance of 5 m from the geophone to get one

simulation as per methodology given by Ryden *et al.* (2004). To get multiple simulations, the head and the geophones were then moved incrementally, keeping the recorder at the same point and then finally, all simulations were joined together to obtain dispersion curve.

All seismic traces obtained from each site were gathered in their acquired order, and the multi-simulated record was compiled to obtain dispersion curves. Finally, the processing of these combined traces was performed using 'Grilla' software, which generates dispersion curves in three variables reflecting the amplitude of signal colour, the phase frequency and phase velocity (Fig. 13). The phase frequency and velocity are the function of wavelength (l) and half of the total wavelength is marked as the penetration depth (Rix and Leipski, 1991). A total of six sites could be covered using the MSOR technique as the rest of the area does not have any linear length, even for a few meters, to get the stiffness values of the near-surface material to invert the HVSR curve. Since the material composition of the slide mass remains the same because the source of material was the same, therefore the data of all HVSR curves falling along section A- A' have been inverted using the dispersion curves from the six sites to obtain 1-D velocity models and to understand the depth of slip surface along this section.

Joint-Fit-Inversion Modeling

Further, forward modelling was carried out to invert HVSR curves using dispersion curves obtained from multiple simulations from different sites. Due to the non-uniqueness issue inherent in H/V inversion, different sets of velocity models can be derived from the same HVSR curves (Sanchez-Sesma, 2017). They can be avoided by joint fit-inversion using initial shear wave velocity information of the surface layer (Pina-Flores *et al.,* 2016) derived from the MSOR technique (Ryden *et al.,* 2004; Harutoonian, 2014; Lin and Ashlock, 2016). Different authors have widely used this methodology in the recent past to allow the derivation of 1-D shear wave velocity profiles of urban sites and slide zones (Castellaro and Mulargia, 2009; Roser and Gosar, 2010; Pina-Flores *et al.,* 2016; Kumar and Mahajan, 2020; Mahajan *et al.,* 2021).

Applying Occam's razor principle, the maximum number of peaks (n) and layers (n+1) was selected to ensure a reliable outcome. The MSOR method initially provided essential information on phase frequency, phase velocity, wavelength (λ), and pseudo-depth from the dispersion curve. Subsequently, in modeling the HVSR curve, details such as the thickness of the initial layers, along with their shear wave velocity and poison ratio, were determined using dispersion curves and material composition data. Further refinement was achieved by utilizing permutation combination methods and incorporating knowledge of shear wave velocity from dispersion curves and layer thickness to model the second contrasting layer obtained from the dispersion curves, specifically for the first HVSR peak. The synthetic HVSR curve derived from the inversion modeling was then matched with average HVSR curves, incorporating initial depth and shear wave velocity constraints. This comprehensive approach enhanced the precision of shear wave velocity profiles, resulting in more accurate analysis outcomes.

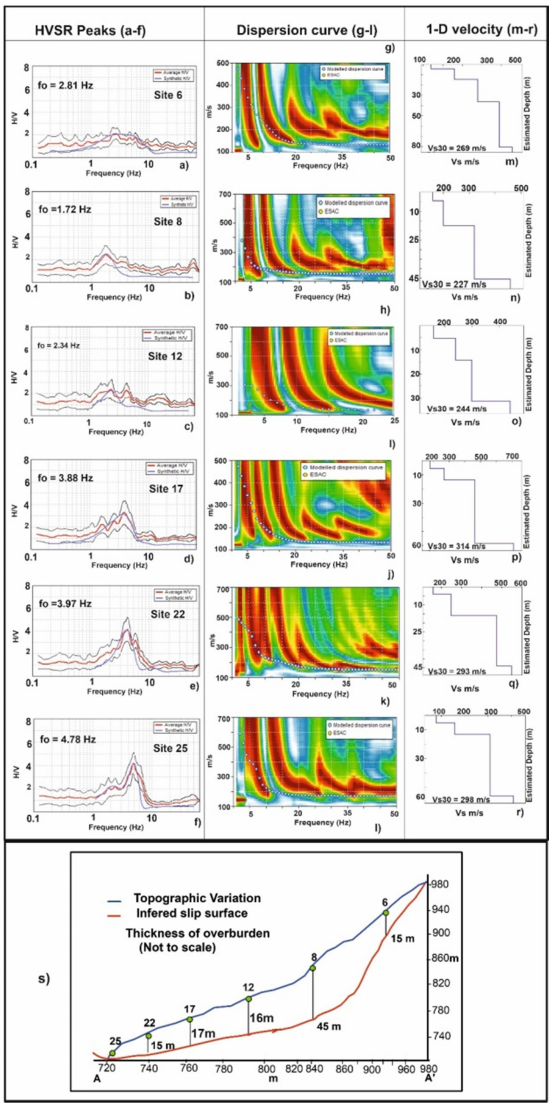

Fig. 14. Shows the HVSR curves (a-f), dispersion curves (g-i) and inverted 1-D shear wave velocity profiles (m-r) for the corresponding HVSR curves and dispersion curves. The lower part of the diagram (s) shows the slip geometry along the A-A' profile for sites no. 6, 8, 12, 17, 22 and 25). The profile A-A' is shown in Fig. 1.

The HVSR curves of sites 6, 8, 17, 22 and 25 have been considered for inverting using corresponding dispersion curves from the same site. The HVSR curves of site 6 and 12 were found to be broad with a peak frequency of 2.81 and 2.34 Hz with a maximum amplitude of 2 and 3, whereas site no. 8 have a peak frequency of 1.78 Hz with a maximum amplitude of 3 (Fig. 11). The sites no. 17, 22 and 25 have 3.88, 3.97 and 4.78 Hz with large amplitude of the order of 4 and 5. Site no. 8 has a lower frequency. Therefore, the estimated depth was also large at that location (i.e. 45 m) compared to other sites. Every site's corresponding 1-D velocity profiles are shown adjacent to the dispersion curve. The final slip surface geometry is shown in Fig. 15s. Sites no. 17, 22 and 25 have high frequency, indicating the presence of stiffer material (may be weather

rock) at a shallower depth, and the same is reflected through the 1-D velocity model. Therefore, the Ambient Noise Measurements coupled with the active seismic method enable us to retrieve the depth of the slip surface, which requires an invasive method using a standard penetration test to understand the variation of thickness of loose sediments above the slip surface (Fig. 14).

MITIGATION MEASURES

Landslides in the Himalayan region can be mitigated through direct and indirect methods. The natural techniques involve implementing physical measures such as erecting retaining walls, reinforced concrete, rock enforcement on slopes, the application of mesh crating, joint repairs using injection grouting material, bioengineering measures, etc. The indirect methods, on the other hand, include drainage improvement, slope geometry modification, terrace farming, etc. The present study areas have a highly rugged terrain with sandy soil and gravelly composition, and multi-directional slope failure; therefore, applying the physical methods mentioned above may not be feasible to mitigate further movement. Under such conditions, the potential of bioengineering has been explored to control erosion in the region. To apply bioengineering measures, it was essential to understand the nature of the soil, its nutrient components and water content. Therefore, soil testing was executed by conducting chemical and grain size analyses of soil samples and geological investigations. This allowed us to identify suitable plant species that can grow effectively to mitigate landmass from further movement (Vasistha *et al.,* 2011 Gray and Leiser, 1982).

Bioengineering techniques offer several advantages over traditional engineering approaches for landslide mitigation. They are often more cost-effective and eco-friendly and provide additional ecological benefits, such as habitat restoration and biodiversity enhancement. Moreover, they can be integrated into the landscape, blending with the natural surroundings and providing long-term sustainability. The selection and design of bioengineering measures for landslide mitigation should consider site-specific existing conditions, such as slope geometry, soil properties, hydrological patterns, and local climate. Proper planning, assessment, and monitoring are crucial to ensure the effectiveness and durability of these techniques in mitigating landslides and promoting slope stability.

The grain size analysis of the slope material indicated that sand constitutes the major portion (60.87 to 92.20%), followed by gravel (14 to 37%) and silt + clay (0.2 to 9%). This composition aligns with the well-graded sand with limited fines and more than 15% gravel, meeting the criteria set by the Indian Standard (IS-1498-1970). The Coefficient of Uniformity and Coefficient of Curvature showed significance in the ranges of 7.5-43.1 and 1.0-2.32, respectively. The soil in the area is sandy, with an organic carbon deficiency ranging from 0.25 to 0.40%

Furthermore, the alkaline nature of the soil is reflected in the pH range of 8.1 to 10.3. Soil nutrient analysis revealed an increasing trend for nitrogen (N) and a decreasing trend for potassium (K), iron (Fe), and zinc (Zn) from the top to the bottom of the landslide zones. Alkaline soil is associated with deficient microbial activity and limited availability of plant nutrients. Additional

soil analysis unveiled low soil organic carbon, phosphorus (P), and manganese (Mn), and high copper (Cu) content. Soil organic carbon content below 1%, along with available soil nitrogen (31.36 to 95.44 kg/ha) and phosphorus (3.57 to 39.06 kg/ha) levels, indicates poor soil quality. Manganese levels ranging from 4.82 to 5.52 ppm and high copper (1.43 to 6.02 ppm) and iron (150 to 617 ppm) content suggest the occurrence of non-saline alkali soils.

The Soldha area, marked by active landslides due to tectonic activity, necessitates landslide disaster risk reduction measures to prevent future property and life loss. Bioengineering emerges as a promising, cost-effective, and environmentally friendly technique compared to conventional civil engineering approaches. The success of bioengineering relies on appropriate vegetation selection, considering edaphic and climatic conditions, slope gradient, and landslide severity. Different landslide zones require distinct risk reduction strategies, considering factors such as depletion and accumulation zones and partially stabilized landslide areas. Best-fit models for observed soil parameters are identified as exponential (N, P, Fe, and Zn) and Gaussian (OC, K, Cu, and Mn), aligning with findings in Tinsukia, Assam, India, by Reza et al. (2019). Strong spatial dependence is observed among certain elements (N, P, Cu, Fe, and Zn), moderate dependence for K and Mn, and weak dependence for organic carbon. These results are consistent with the findings of Kumar *et al.* (2021)

A bioengineering technique has been proposed to stabilize the Soldha slide zone, considering grain size analysis and soil chemical parameters. This study allows us to carefully identify different plant species at the depletion and accumulation zones. The slope stability can significantly be enhanced if the plantation is planned strategically, considering the unique characteristics of the slide zones and soil parameters to mitigate the risk associated with landslide movement and erosion along gullies.

The mitigation measures for promoting stabilization in such areas require mulching treatment, which involves establishing vegetative cover by planting grass, shrubs on the denudated slopes faces, waterlogged areas and exposed debris material which contains organic material from the eroded plantation/grasses. Further broadcasting of seeds of the local habitation, shrubs, trees, grasses and climbers can further enhance the management of small or creep movements due to slope and loose soil material. One can arrest soil erosion by implementing small preliminary approaches, and organic matter, which has a fragile concentration in the soil, can be restored.

This technique will allow us to know the water retention capacity at the surface, which otherwise penetrates down due to the sandy composition of the slide zone. Further, a slight modification of slopes, reshaping small gullies by establishing vegetation through mulching treatment, could stabilize such areas, protect against soil erosion and allow small grasses to grow.

The central section of the Soldha slide zone comprises displaced rock fragments of sandstone from the crown and western parts, forming debris above the bedrock. To foster ecological balance, local and native trees such as Agave, Lannia, Ipomeia, Jatropha, Anthrocephalus, Erythrina, etc., are recommended for plantation on the

downhill side. These trees play a crucial role in preventing further gully erosion in the slide areas. Deep-rooted trees contribute to slope stability at varying angles. Following the stabilization of the landslip with grasses and shrubs, the planting of local native tree seedlings along the landslide contour becomes crucial to shield the soil from the adverse effects of rainfall.

The angle of slope during tree plantation significantly influences reinforcement effectiveness. Research by Lan *et al.* (2020) indicates that slope angles of 20-35° demonstrate superior sediment interception, hindering sediment slide and collapse compared to angles of 50 to 60°. Given the high porosity of the slide and the accumulation of fine clay and silt near the slip surface, enhancing the soil's water-holding capacity on the top becomes imperative. Specifically selected plant species are needed to achieve this objective effectively. Additionally, deep-rooted broad-leaf plants can reduce water content through transpiration in the central and toe areas, mitigating waterlogging and slip surface movement.

Due to the slide's high surface soil porosity, a significant amount of water penetrates up to the slip surface, facilitating landmass movement. To address this, the proposed species listed in Table 2 are recommended for planting along the slide zones. These species aim to increase water-holding capacity at the surface and decrease water content at the slip surface, contributing to enhanced slope stability.

Table 2. List of plant species suggested for planting at Soldha Landslide

Sr. no.	Botanical name	Local name	Sr. no.	Botanical name	Local name
A. Grass species			21	*Terminalia bellirica*	Behada
1	*Eulaliopsis binata*	Bhabar, Bagar	22	*Phyllanthus emblica*	Amla
2	*Hetropogon contortus*	Lambu	23	*Pinus roxburghi*	Chir Pine
3	*Sorghum nitidum*	Lunji	24	*Morus alba*	Mulberry
4	*Cenchrus purpureus*	Napier	25	*Ficus roxburghi*	Trimbal
5	*Cynodon dactylon*	Dhoob	26	*Diospyros melanoxylon*	Kendu
6	*Tripidium bengalense*	Munj	27	*Grewia optiva*	Beul
7	*Dendrocalamus strictus*	Bamboo	28	*Pyrus pashia*	Kainth
B. Tree species			29	*Acacia catechu*	Khair
1	*Bauhinia variegata*	Kachnar, Karal	30	*Cassia fistula*	Kener
2	*Terminalia bellirica*	Bahera	31	*Celtis australis*	Khidak
3	*Cordia dichotoma*	Lasura	32	*Pistacia integerrrima*	Kaakarasingi
4	*Butea monosperma*	Dhak, Plah	33	*Toona ciliata*	Toon
5	*Dalbergia sissoo*	ShishamTali	34	*Melia azadirachta*	Derech

Sr. no.	Botanical name	Local name	Sr. no.	Botanical name	Local name
6	*Acacia nilotica*	Kikar	C. Shrub species		
7	*Albizia lebbeck*	Siris, Sarin	1	*Vitex negundo*	Bana
8	*Albizia procera*	Siris	2	*Dodonaea viscosa*	Maindhor
9	*Morus alba*	Tut	3	*Punica granatum*	Anar, Doran
10	*Syzygium cumini*	Jaman	4	*Zizyphus jujuba*	Ber
11	*Tamarandus indica*	Imli	5	*Agave americana*	Ram ban
12	*Terminalia arjuna*	Arjun	6	*Flemingia semialata*	Bara Solpan
13	*Azadrichta indica*	Neem	7	*Opuntia ficus india*	Kaiktus
14	*Prosopis juliflora*	Khehri	8	*Adhatoda vasica*	Basuti
15	*Moringa olifera*	SananSuhanjua	9	*Carissa carandas*	Karonda
16	*Bombex ceiba*	Semul	10	*Lawsonia inermis*	Hina
17	*Sesbania sesban*	Jayantika	11	*Muraya cunningham*	Curry Leaves
18	*Wendlandia grandis*	Panshera	12	*Berberis aristata*	Chitra
19	*Mallotus philippines*	Kamala Tree	13	*Ipomea fistula*	Morning Glory
20	*Lannea coromandelica*	Indian Ash Tree	14	*Woodfordia fruticosa*	Dhawi

RESULTS AND DISCUSSION

The Soldha slide zone was triggered in October 2013 due to continuous rainfall in the preceding months, resulting in the downslope movement of the entire land mass by 40-60 m (Randhwava and Dhar 2013). Located on the hanging wall of Jawalamukhi Thrust, the area encounters slight movements attributable to ongoing tectonic disturbances. Characterized by high rainfall and a highly porous surface layer, the zone allows water to percolate deeply into the subsurface, potentially inducing movement along the slip surface. The rainfall analysis suggests a gradual slope failure attributed to the progressive reduction in shear strength of the predominantly sandy slope material followed by high-intensity rainfall in October 2013. The continuous downslope movement was instigated by heightened shear stress on the slip surface in the middle section of the landslide body. Moreover, removing the upslope toe (now forming the crown of the Soldha landslide) contributed to its further sliding.

The rotational nature of the slide, with varying slip depths and the presence of multidirectional joints and weathered rock material, indicates the rate of weathering. The slope angle, ranging from over 65° near the crown to gentle to moderate slopes at the centre and toe area, further influences the slide's dynamics.

Field investigations and hypsometer analysis by Sharma and Mahajan (2018) revealed high drainage density, signifying immature geomorphic features. The debris formed from Middle Siwalik sandstone rock fragments

contributes to the rugged terrain of the slide zones. The area is characterized by gorges, depressions, and ridges, underlain by claystone and mudstone layers. The investigation supports a multidirectional slide movement, particularly in the southwest-eastern and southern directions.

The topsoil, comprising rock fragments and debris material, is sandy and highly porous, impeding water retention. The fine soil exists at deeper depths, creating an impermeable lower layer that facilitates moisture movement. Grain size analysis by Mahajan et al. (2022) revealed well-graded sand, gravel, and silt + clay components, with soil characteristics indicating alkalinity, deficient humus, and poor nutrient levels.

The analysis shows multidirectional joints indicating the complexity of the area (Fig. 6). The principal direction of the joint is either in the western or northern exposure, indicating the presence of stresses from the northeast-southwest or east-west, reflecting the role of both longitudinal and transverse features in the development of strains in the region. The multiple directional developments of joints reflect the level of stresses in the area that might lead to crown failure, and the gravity of the material allows its movement along the slip surface due to the increased water content.

The application of LiDAR has been increasing for landslide investigations (Derron and Jaboyedoff 2010; Heritage and Large (2009), and our experimental investigations on the Soldha slide zone also reveal southeastward movement during the 2023 monsoon season and the rate of movement noticed using LiDAR vary from 0.032m in the northwest side to 0.398 m in the south-eastern direction in 44 hrs at point locations 5, 9 and 1(Fig.8). Further studies are required from the same region with month-long observation to establish its subsequent effects on the Niangal village for rescue measures.

The examination of HVSR curves reveals two distinct typologies of HVSR curves from the Soldha slide zone, i.e., multiple and precise peak curves. The clear HVSR peak is prominently observed from the slide zone's central part, indicating a sharp contrast between the underlying bedrock and overlying debris material (Fig. 14; site no. 3, 5 and 9). Other sharp peaks are observed in sites 22, 24 and 25 (Fig.12), located near the first scarp and crown part, with thin sediment cover above bedrock, reflecting sharp impedance contrast among the overlying layer and underlying very stiff material (f0 = 3 and 4 Hz). On the other hand, regions lying on the sloping interface are represented by multiple peak curves reflecting complex wave field patterns owing to the shallow structures with weak impedance contrast (i.e. site no. 3, 5 and 6; Fig. 11). Some of the HVSR peaks have very low amplitude, which may reflect very week contrast between the overlying debris and underlying stiff material. In general, the predominant frequencies are highly variable, with the dominance of high fundamental frequency (2-5 Hz) in the northern and western parts.

In contrast, low-frequency peaks are prominent from the central part of the Soldha slide zone, which has thick debris material. The HVSR peaks provide valuable information on the fundamental frequency of any soil site; however, to determine the thickness of any site, one should know the shear wave velocity or stiffness values of that site to calculate the thickness of sediments above the bedrock. Kramer (1996) has suggested a formula

to derive the thickness of deposits (H), which is a function of the shear wave velocity (Vs) and fundamental frequency (f0).

4H= Vs/f0 ------1

The question arises about calculating shear wave velocity in hilly terrain and from a slide zone. To achieve the required target, two different seismic methods (HVSR and MASW) have been used to independently cross-check and validate their outcome and ensure the reliability and accuracy of the results.

Further, the analysis of results from ambient noise measurements allowed information on the depth of the slip surface and shear wave velocity to be obtained by inferring the geometrical reconstruction of the noise recording along the profile. This information reveals the impedance contrast between the sliding body and the bedrock. The 1-D Vs profiles provide the shear wave velocity of the material involved in the gravity movement of the subsurface material. The HVSR spectra provide significant resonance peaks with a frequency range from 1.88-5 Hz, and amplitude varies in general 2-3. It goes up to 5 near the toe zone, possibly due to the transition between the landslide mass and the bedrock material. The directional component observed at different sites indicated multidirectional behaviour of slide mass. Various authors have also observed it while conducting such experiments in other parts of the world (Del Gaudio et al. 2013) Spudich et al. 1996). The surface material up to a few meters has shallow shear wave velocity (Vs = 200-250m/s), which is involved in the landslide mass. In contrast, it has increased (Vs-500-600m/s) at a depth of 40-45 m, which can be due to the presence of very stiff material or bedrock (Fig. 12,13 & 14) and considered as a transition between the surface material and bedrock.

The overall evaluation of the Soldha slide zone using various geological and geotechnical geophysical geochemical analyses reveals the soil's suitability for deep-root plant species, promoting vegetation growth and aiding in limiting water movement downward as the shear strength of the material increasing with depth as reflected in Vs profiles. Chemical analysis and grain size analysis emphasize the soil's dependency on ions, highlighting the spatial solid dependence of soil. The proposed application stabilizes the slide zones and contributes to ecosystem maintenance, carbon pool improvement, and global warming mitigation. To ensure stabilization, native plant species should be introduced, and invasive species with root-binding properties can be strategically utilized. The bioengineering approach, involving earth balls, seed broadcasting, or slip planting, offers a sustainable solution for stabilizing the slide zone and enhancing surface soil water-holding capacity, fostering ecological balance.

CONCLUSION

In the present study, the Soldha slide zone was studied using different geological and geophysical methods to understand the behaviour of the soil, its grain size distribution, water retention capability, and shear strength of the slide zone with depth. The grain size analysis suggested a high percentage of gravel and a meagre percentage of fine clay at the surface. High rainfall and a porous surface layer facilitate water percolation into the subsurface, potentially triggering movement along the slip surface. The

joint analysis and field observations underscore the complexity of the Soldha slide zone and its susceptibility to varied triggers and directional movements. The rotational nature of the slide is evident, with varying slip depths from 15 to 45 m at the top to the centre and 12 to 15 m at the toe area, influenced by multidirectional joints, weathered rock material, and slope angles. Ambient noise analysis was conducted from 30 sites, and their analysis suggests that the slide is multidirectional. The Lidar survey further revealed significant movement towards the southeast direction. Nutrient analysis indicates deficiencies in humus, low organic carbon, phosphorus, manganese, and high copper and iron content. Soil organic carbon content is below 1%, and available soil nitrogen and phosphorus indicate poor soil quality. Considering the ongoing slide movement, depth of slip surface, and grain size analysis, the suggested plantation needs to be encouraged apart from stabilizing the slope from the toe area. According to the study, ambient noise measurements coupled with a Lidar survey, grain size analysis, joint analysis and geochemical analysis have provided a comprehensive approach for landslide assessment and mitigation.

ACKNOWLEDGEMENT

The authors thank the central University of Himachal Pradesh University authorities for providing logistic support for conducting this research. There was no funding source for this research. The authors thank the Department of soils Sciences, CSK Himachal Krishi Vishvavidyalaya (CSK HPKV) Palampur for conducting the soil sampling from Soldha slide zones and their analysis. The authors also acknowledge the M/s Meatech Solutions, Gurgaon for conducting experimental LiDAR survey.

Statement and declaration

Funding: The authors did not receive any grant for financial aid from any organisation for carrying out this research work.

Competing Interest: The authors declares that there is no competing interest

Author's contribution: All the authors contributed to the study conception design, analysis, and interpretation.

REFERENCES

Ambraseys, N. and Bilham, R. 2000. A note on the Kangra Ms 7.8 Earthquake of 4 April 1905. *Current Science*, **79**: 101–106.

Amitrano, D., Gaffet, S., Malet, J. P. and Maquaire, O. 2007. Understanding mudslides through micro-seismic monitoring: the Super-Sauze (South-East French Alps) case study. Bulletin de la Soci´et´e G´eologique de France **178**: 149–157. https://doi.org/10.2113/gssgfbull.178.2.149.

Anbalagan, R. 1992. Landslide hazard evaluation and zonation mapping in mountainous terrain. *Eng. Geol.* **32**(4):269–277

Bontemps, N., Lacroix, P., Larose, E., Jara, J. and, Taipe, E.2020. Rain and small earthquakes maintain a slow-moving landslide in a persistent critical state. *Nat Commun* **11**: 1–10. https://doi.org/10.1038/s41467-020-14445-3.

Burjanek, J., Gassner-Stamm, G., Poggi, V., Moore, J. R. and Fah, D. 2010. Ambient Vibration Analysis of an Unstable

Mountain Slope. *Geophysical Journal International* **180**: 820–828.

Carri`ere, S.R., Jongmans, D., Chambon, G., Bi`evre, G. Lanson, B. Bertello, L. Berti, M. Jaboyedoff, M. Malet, J.-P. and Chambers, J. E. 2018. Rheological properties of clayey soils originating from flow-like landslides. Landslides **15**: 1615–1630. https://doi.org/10.1007/s10346-018-0972-6.

Carter, W., Shrestha, R., Tuell, D., Bloomquis,t D. and Sartori, M. 2001. Airborne laser swath mapping shines new light on earth's topography. *Eos, Trans, Am Geophys Union* **82**(46):549, 550, 555

Castellaro, S. and Mulargia, F. 2009. Vs30 estimates using constrained H/V measurements. *Bull Seismol Soc Am* **99** (2A):761–773.

Danneels, G., Bourdeau, C., Torgoev, I. and Havenith, H.B. 2008. Geophysical investigation and dynamic modeling of unstable slopes: case-study of Kainama (Kyrgyzstan). *Geophys J Int* **175**: 17–34.

https://doi.org/10.1111/j.1365-246X.2008.03873.x.

Del Gaudio, V., Muscillo, S., Wasowski, J. 2014. What we can learn about slope response to earthquakes from ambient noise analysis: An overview. *Engineering Geology*, Special Issue on The Long-Term Geologic Hazards in Areas Struck by Large Magnitude Earthquakes **182**: 182–200. https://doi.org/10.1016/j.enggeo.2014.05.010.

Fiolleau, S., Jongmans, D., Bi`evre, G., Chambon, G., Baillet, L. and Vial, B. 2020. Seismic characterization of a clay-block rupture in Harmali`ere landslide, French Western Alps. Geophysical Journal International **221**: 1777–1788. https://doi.org/10.1093/gji/ggaa050

Gray D.H. and Leiser A.T. 1982. Role of Vegetation in the Stability and Protection of Slopes. In: Gray, D.H. and Leiser, A.T. (eds.), Biotechnical Slope Protection and Erosion Control. (New York: Van Nostrand Reinhold Company Inc., 1982), pp. 37-65.

Guillemot, A., Helmstetter, A., Larose, E., Baillet, L., Garambois, S., Mayoraz, R. and Delaloye, R. 2020. Seismic monitoring in the Gugla rock glacier (Switzerland): ambient noise correlation, microseismicity and modeling. *Geophys J Int* **221**: 1719–1735. https://doi.org/10.1093/gji/ggaa097.

Harutoonian, P., Leo C. J., Doanh, T., Castellaro, S., Zou, J.J. Liyanapathirana, D.S. Wong, H. and Tokeshi, K. 2014. Microtremor measurements of rolling compacted ground. *Soil Dyn. Earthq. Eng.* **41**: 23–31. https://doi.org/10.1016/j.soildyn.2012.05.006.

Haugerud, R. A., Harding, D. J., Johnson, S.Y., Harless, J. L., Weaver, C.S. and Sherrod, B.L. 2003. High-resolution lidar topography of the Puget Lowland, Washington—A Bonanza for earth science. GSA Today **13**:4–10

Hausler, M., Michel, C., Burj´anek, J. and Fah, D. 2019. Fracture Network Imaging on Rock Slope Instabilities Using Resonance Mode Analysis. Geophysical Research Letters **46**: 6497–6506. https://doi.org/10.1029/2019GL083201.

Imposa, S., Grassi, S., Fazio, F., Rannisi, G. and Cino, P. 2017. "Geophysical Surveys to Study a Landslide Body (North-Eastern Sicily)." *Natural Hazards* **86**: 327–343.

Jaboyedoff, M., Oppikofer, T., Locat, A., Locat, J., Turmel, D., Robitaille, D., Demers, D., Locat, P. 2009. Use of ground-based LIDAR for the analysis of retrogressive landslides in sensitive clay and of rotational landslides in river banks. *Can Geotech J* **46**:1379–1390. doi:10.1139/T09-073

Jackson, M. L. 1973. Soil chemical analysis. Prentice Hall of India. Pvt. Ltd., New Delhi. pp. 498.

Jongmans, D. and Garambois, S. 2007. Geophysical investigation of landslides: a review. Bulletin de la Soci´et´e G´eologique de France 178, 101–112. https://doi.org/10.2113/ gssgfbull.178.2.101.

Kleinbrod, U., Burj´ anek, J., F¨ ah, D. 2019. Ambient vibration classification of unstable rock slopes: A systematic approach. Engineering Geology **249**: 198–217.

https://doi.org/10.1016/j.enggeo.2018.12.012.

Kumar, P., Kumar, P. and Shukla, A.K. 2021. Spatial Modeling of Some Selected Soil Nutrients Using Geostatistical Approach for Jhandutta Block (Bilaspur District), Himachal Pradesh, India. *Agric Res* **10:** 262–273. https://doi.org/10.1007/s40003-020-00494-z

Kumar, S. and Mahajan, A.K. 2001. Seismotectonics of the Kangra region, Northwest Himalaya. Tectonophysics, **331** (4): 359-371

Kumar, P., Meena N.K. and Mahajan A.K. 2019. Major ion chemistry, catchment weathering and water quality of Renuka Lake, north-west Himalaya, India. *Environ Earth Sci* **78**:319. https://doi.org/10.1007/s12665-019-8315-z

Kramer, S.L. 1996. Geotechnical Earthquake Engineering, Ed. Prentice Hall. Upper Saddle River, New Jersey; pp 653

Larose, E. Carri`ere, S., Voisin, C., Bottelin, P., Baillet, L., Gu´eguen, P., Walter, F., Jongmans, D., Guillier, B., Garambois, S., Gimbert, F. and Massey, C. 2015. Environmental seismology: What can we learn on earth surface processes with ambient noise? *Journal of Applied Geophysics* **116**: 62–74. https://doi.org/10.1016/ j.jappgeo.2015.02.001.

Lan, H., Daojie W., Songtang He, Yinghcao F., Wenle C., Peng Z., Yuchao Qi. 2020. Experimental study on the effects of tree planting on slope stability Landlsides **17**(1): 1021-1035 DOI: 10.1007/s10346-020-01348-z

Le Breton, M. 2019. Suivi temporel d'un glissement de terrain `a l'aide d''etiquettes RFID passives, coupl´e `a l'observation de pluviom´etrie et de bruit sismique ambiant — chapter 8 — Impulse response from rainfall to displacement (PhD Thesis). Universit´e Grenoble Alpes, ISTerre, Grenoble, France.

Lin, S. and Ashlock, J.C. 2016. Surface-wave testing of soil sites using multichannel simulation with one-receiver. *Soil. Dyn. Earthq. Eng.* **87**: 82–92. http://dx.doi.org/10.1016/j.soildyn.2016.04.013.

Lindsay, W. L., & Norvell, W. A. 1978. Development of a DTPA soil test for zinc, iron, manganese and copper. *Soil Science Society of America Journal*, **42**(3): 421–

428. https:// doi. org/ 10. 2136/ sssaj 1978.03615 99500 42000 30009x

Mahajan, A.K., Kumar, P. and Kumar, P. 2021 Near-surface seismic site characterization using Nakamura-based HVSR technique in the geological complex region of Kangra Valley, northwest Himalaya, India. *Arabian Journal of Geosciences*, **14**: 826. https://doi.org/10.1007/s12517-021-07136-w

Mahajan, A.K., Sharma, S., Patial, S., Sharma, H. and Negi, S. 2022. A brief address of the causal factors, mechanisms, and the effects of a major landslide in Kangra valley, North-Western Himalaya, India. *Arabian Journal of Geosciences* **15**:925 https://doi.org/10.1007/s12517-022-10163-w

Mahajan, A.K. Thakur, V.C., Sharma, M.L. and Chauhan, M. 2010. Probabilistic seismic hazard map of NW Himalaya and its adjoining area, India. Nat Hazards **53**: 443–457

M´eric, O., Garambois, S., Malet, J.P., Cadet, H., Gu´eguen, P. and Jongmans, D. 2007. Seismic noise-based methods for soft-rock landslide characterization. Bulletin de la Soci´et´e G´eologique de France **178**: 137–148. https://doi.org/10.2113/gssgfbull.178.2.137.

Nakamura, Y. 1989. A method for dynamic characteristics estimation of subsurface using microtremor on the ground surface. Quarterly Report of the Railway Technical Research Institute **30**: 25–33.

Narula, P.L. and Shome, S.K. 1992. Macroseismic studies of recent earthquakes in northwest Himalaya- a review. Current Science **62**(1&2): 24–33

Olsen, R. S. 1954. Estimation of available phosphorus in soils by extraction with sodium bicarbonate (USDA Circular No. 939). Washington, D.C.: U.S. Government Printing Office.

Patial, S., Mahajan, A.K., Sharma, H., and Negi, S. 2023. Evaluation of landslides using ambient noise measurements: A case study of Soldha Landslide, Northwest Himalaya, India. Arabian *Journal of Earth Sciences* **16**: 449-469 https://doi.org/10.1007/s12517-023-11537-4.

Pazzi, V., Tanteri, L., Bicocchi, G. D., Ambrosio M., Caselli A. and Fanti R. 2017. H/V measurements as an effective tool for the reliable detection of landslide slip surfaces: Case studies of Castagnola (La Spezia, Italy) and Roccalbegna (Grosseto, Italy). *Physics and Chemistry of the Earth* **98**:136-153.

Pina-Flores, J., Perton, M., García-Jerez, A., Carmona, E., Luzón, F., Molina-Villegas, J.C. and Sanchez-Sesma, F.J. 2016. The inversion of spectral ratio H/V in a layered system using the diffuse field assumption (DFA). *Geophys. J. Int.* **208**: 577–588. https://doi.org/10.1093/gji/ggw416.

Reza, S.K., Dutta, D., Bandyopadhyay, S. and Singh, S.K. 2019. Spatial variability analysis of soil properties of Tinsukia District, Assam, *India. Agricultural Research* **8** (2): 231–238

Rezaei, S., Choobbasti, A.J. and Kutanaei, S.S. 2013. Site effect assessment using microtremor measurement, equivalent linear method, and artificial neural

network (case study: Babol, Iran). *Arab. J. Geosci.* **8**(3): 1453–1466. https://doi.org/10.1007/s12517-013-1201-1.

Rezaei, S. and Choobbasti. A. J. 2017. Application of the Microtremor Measurements to a Site Effect Study." *Earthquake Sciences* **30**: 157–164. doi:10.1007/s11589-017-0187-2.

Rix, G. J. and Leipski, E. A. 1991. Accuracy and resolution of surface wave inversion. In: Bhatia SK, Blaney GW (eds) Recent advances in instrumentation, data acquisition and testing in soil dynamics. *American Society of Civil Engineers*, Reston, pp 17–32

Roser, J. and Gosar, A. 2010. Determination of Vs_{30} for seismic ground classification in the Ljubljana area, Slovenia. *Acta. Geotech. Slov.* **7**: 61–76.

Ryden, N., Park, C.B., Ulriksen, P. and Miller, R.D. 2004. Multimodal approach to seismic pavement testing. *J. Geotech. Geoenvironmental Eng.* **130**: 636–645. https://doi.org/10.1061/(ASCE)1090-0241(2004)**130**:6(636).

Sharma, S. and Mahajan, A.K. 2018. Comparative evaluation of GIS-based landslide susceptibility mapping using the statistical and heuristic approach for Dharamshala region of Kangra Valley, India. Geoenvironmental Disasters. https://doi.org/10.1186/S40677-018-0097

Sharma, S. and Mahajan, A.K. 2020. GIS-based sub-watershed prioritization through morphometric analysis in the outer Himalayan region of India. *Appl Water Sci.* **10**: 163. https://doi.org/10.1007/s13201-020-01243-x

Sanchez-Sesma, F. J. 2017. Modeling and inversion of the microtremor H/V spectral ratio: physical basis behind the diffuse field approach. *Earth Planets and Sp.* 69–92. https://doi.org/10.1186/s40623-017-0667-6.

Sens-Sch¨onfelder, C. Brenguier, F. 2019. Noise-Based Monitoring, in: Seismic Ambient Noise. Cambridge University Press

SESAME 2004. Guidelines for the Implementation of the H/V Spectral Ratio Technique on Ambient Vibrations: Measurements, Processing and Interpretation. SESAME European Research Project WP12, deliverable D23.12; http://sesame-fp5.obs.ujf-grenoble.fr/

Singh, S., Joshi, A., Sahu A., Prasath R. A., Shrma S. and Dwivedi C.S. 2022. Himalayan Landslides–Causes and Evolution. Disaster Management in the Complex Himalayan Terrains. ISBN : 978-3-030-89307-1

Singh, T. and Awasthi, A. K. 2019. Deformation in the Kangra Reentrant, Himachal Pradesh of NW-Sub Himalaya of India: a paradox. In Tectonics and Structural Geology: Indian Context: 381–396).

Slob, S. and Hack, R. 2004. 3D terrestrial laser scanning as a new field measurement and monitoring technique. In: Engineering geology for infrastructure planning in Europe: a European perspective, Lectures Notes in Earth Sciences, Springer, Berlin/Heidelberg, **104:**179–189.

Slob, S., Hack, H. and Turner, A. K. 2002. An approach to automate discontinuity measurements of rock faces using laser scanning techniques. In: Dinid da Gama

C, Riberia e Sousa L (eds) Proceedings of ISRM EUROCK 2002, 25–28 November 2002, Funchal, Portugal, Sociedade Portuguesa de Geotecnia, pp 87–94

Subbiah, B. V. and Asija, G. L. 1956. A rapid procedure for estimation of available nitrogen in soils. *Current Science,* **25**: 259–260.

Thakur, V.C., Joshi, M, Sahoo, D., Suresh, N., Jayangondapermal, R. and Singh A. 2014. Partitioning of convergence in northwest sub-Himalaya: estimation of late Quaternary uplift and convergence rates across the Kangra reentrant, North India. *Int J Earth Sci* **103**:1037–1056.

Vashistha HB, Rawat A, Soni P (2011) Hazard Mitigation through the application of Bioengineering in landslide Areas: a Case Study of Varunavat Landslide, Uttarkashi (Uttarakhand). Disaster and Development **5**(1&2):37–52

Walkley, A. and Black, I. A. 1934. An examination of the Degtjareff method for determining soil organic matter, and a proposed modification of the chromic acid titration method. *Soil Science,* **37**: 29–38.

Whiteley, J.S., Chambers, J.E., Uhlemann, S., Wilkinson, P.B. and Kendall, J.M. 2019. Geophysical Monitoring of Moisture-Induced Landslides: A Review. Reviews of Geophysics **57**: 106–145. https://doi.org/10.1029/2018RG000603.